Appendix B

APPENDIX B: ADDITIONAL FIGURES

B.1. *Implementation details*

B.1.1. *Bonferroni confidence set*

This section describes the implementation of the Bonferroni-type method proposed by Moon et al. (2013). The following algorithm is a variation of the algorithm outlined on p.17 in Moon et al. (2013). There is one minor difference between the algorithms. To avoid dealing with degenerate $\hat{D}$, we add Step 3.c instead of implicitly adjusting the criterion function as proposed in Section 4.2 of Moon et al. (2013). The rate of the sequence $\underline{\sigma}_T$ guaranties that the additional noise $\underline{\sigma}_T \epsilon_b$ does not affect the asymptotic distribution of $\mathcal{G}(\xi_g)$.

1. Generate N_B draws $\left\{\mu_b^*\right\}_{b=1}^{N_B} \sim N\left(\widehat{\mu}_T, \widehat{\Omega}_T\right)$.
2. Generate N_G grid points $\{x_g\}_{g=1}^{N_g}$ on a unit $d-$sphere distributed uniformly using the algorithm from Uhlig (2005).
3. For every grid point x_g, we implement the following statistical test (of size $1-\alpha/2$) of whether $B_{1g} = \widehat{\Sigma}_T^{1/2} x_g$ satisfies all identification restrictions. This is done by following Steps a) to g) below.
   (a) Compute estimated residuals[24],
   $$\xi_g = \left(S'\left(\hat{\mu}_T\right), Z'\left(\hat{\mu}_T\right)\right)' B_{1g}.$$
   (b) Compute re-centered bootstrap residuals $\left\{\xi_{g;b}^*\right\}_{b=1}^{N_B}$,
   $$\tilde{\xi}_{g;b}^{\star} = \left(S'\left(\mu_b^*\right), Z'\left(\mu_b^*\right)\right)' \Sigma_b^{*1/2} x_g - \xi_g.$$
   (c) Add independent normally distributed noise with $\epsilon_b \sim N(0, I)$ and $\underline{\sigma}_T = 10^{-6}/\sqrt{T \ln(\ln T)}$,
   $$\xi_{g;b}^* = \tilde{\xi}_{g;b}^{\star} + \underline{\sigma}_T \epsilon_b.$$
   (d) Compute standard errors for $\left\{\xi_{g;b}^*\right\}_{b=1}^{N_B}$. The diagonal matrix $\hat{D}^{1/2}$ has the corresponding standard errors on the diagonal.
   (e) Select binding inequities as inequalities corresponding to the components ℓ of ξ_g such that
   $$e_\ell' \hat{D}^{-1/2} \xi_g \leq \kappa_T = 1.96 \ln(\ln T).$$
   (f) Compute the criterion function $\mathcal{G}(\xi_g)$ and $\left\{\mathcal{G}\left(\xi_{g;b}^*\right)\right\}_{b=1}^{N_B}$ which includes only the equalities and the binding inequalities, where
   $$\mathcal{G}\left(\xi_{g;b}^*\right) = \sum_{\ell=1}^{m_z} \left(e_\ell' \hat{D}^{-1/2} \xi_{g;b}^*\right)^2 + \sum_{\ell=m_z+1}^{m_s+m_s} \left(e_\ell' \hat{D}^{-1/2} \xi_{g;b}^*\right)^2 \mathbf{1}\left\{e_\ell' \hat{D}^{-1/2} \xi_g \leq \kappa_T\right\} \tag{B.1}$$
   (g) Grid point x_g passes the test if $\mathcal{G}(\xi_g)$ is less that $1-\alpha/2$ sample quantile of $\left\{\mathcal{G}\left(\xi_{g;b}^*\right)\right\}_{b=1}^{N_B}$.
4. If x_g passes the test in Step 3, compute $\underline{\lambda}_{k,i,j}^{(g)}$ and $\bar{\lambda}_{k,i,j}^{(g)}$ as $\alpha/4$ and $1-\alpha/4$ sample quantiles of $\left\{e_i' C_k\left(A_b^*\right)\sqrt{\Sigma_b^*} x_g\right\}_{b=1}^{N_B}$ correspondingly. Otherwise set $\underline{\lambda}_{k,i,j}^{(g)} = +\infty$ and $\bar{\lambda}_{k,i,j}^{(g)} = -\infty$.
5. Report
$$\mathrm{CS}_T^{MSG}(1-\alpha) = \left[\min_{g=1,N_G} \underline{\lambda}_{k,i,j}^{(g)}, \max_{g=1,N_G} \bar{\lambda}_{k,i,j}^{(g)}\right].$$

[24] We only compute matrices $\left(S'\left(\hat{\mu}_T\right), Z'\left(\hat{\mu}_T\right)\right)' \sqrt{\widehat{\Sigma}_T}$ and $\left(S'\left(\mu_b^*\right), Z'\left(\mu_b^*\right)\right)' \sqrt{\Sigma_b^*}$ once to speed up the costly matrix multiplication.

Our implementation corresponds to a generalized version of the criterion function considered in Section 6 of Moon et al. (2013). This generalized criterion function can potentially be applied to a combination of zero and sign restrictions. In our baseline empirical application, however, the acceptance rate of Step 3 is so low that we could not find a single point out of 10000 grid points that would pass the test. For this reason, we report the results for the alternative identification scheme with the zero restriction on the FFR being replaced by a negative sign restriction.

The number of grid points that passes Step 4 of the algorithm depends crucially on the number of the identifying restrictions imposed. In our experiment, every additional sign restriction reduces the acceptance rate almost by half and, correspondingly, requires twice more grid points and computational time to achieve the same level of accuracy. For the UMP example with 4 sign restrictions the acceptance rate is 9.1%.

B.1.2. *Joint Confidence Sets*

To implement Inoue and Kilian (2013)'s algorithm, we first sample 10,000 joint draws from the posterior of reduced-form parameters and structural coefficients that satisfy all identification restriction. We use those draws to compute 10,000 structural impulse response function. Second, we sample 20,000 draws of reduced-form parameters to compute the marginal posterior density for each structural response. Third, we compute a joint 68% credible set by keeping all of structural responses which have marginal density higher than the lowest 32%. The second step is computationally costly. In our implementation it takes 2.5 hours when using 50 parallel workers in Matlab.

Figure 5: Robust Bayesian credibility of the delta-method interval based on the posterior distribution $\mu^* \sim \mathcal{N}(\widehat{\mu}_T, \widehat{\Omega}_T/T)$, $T = 342$.

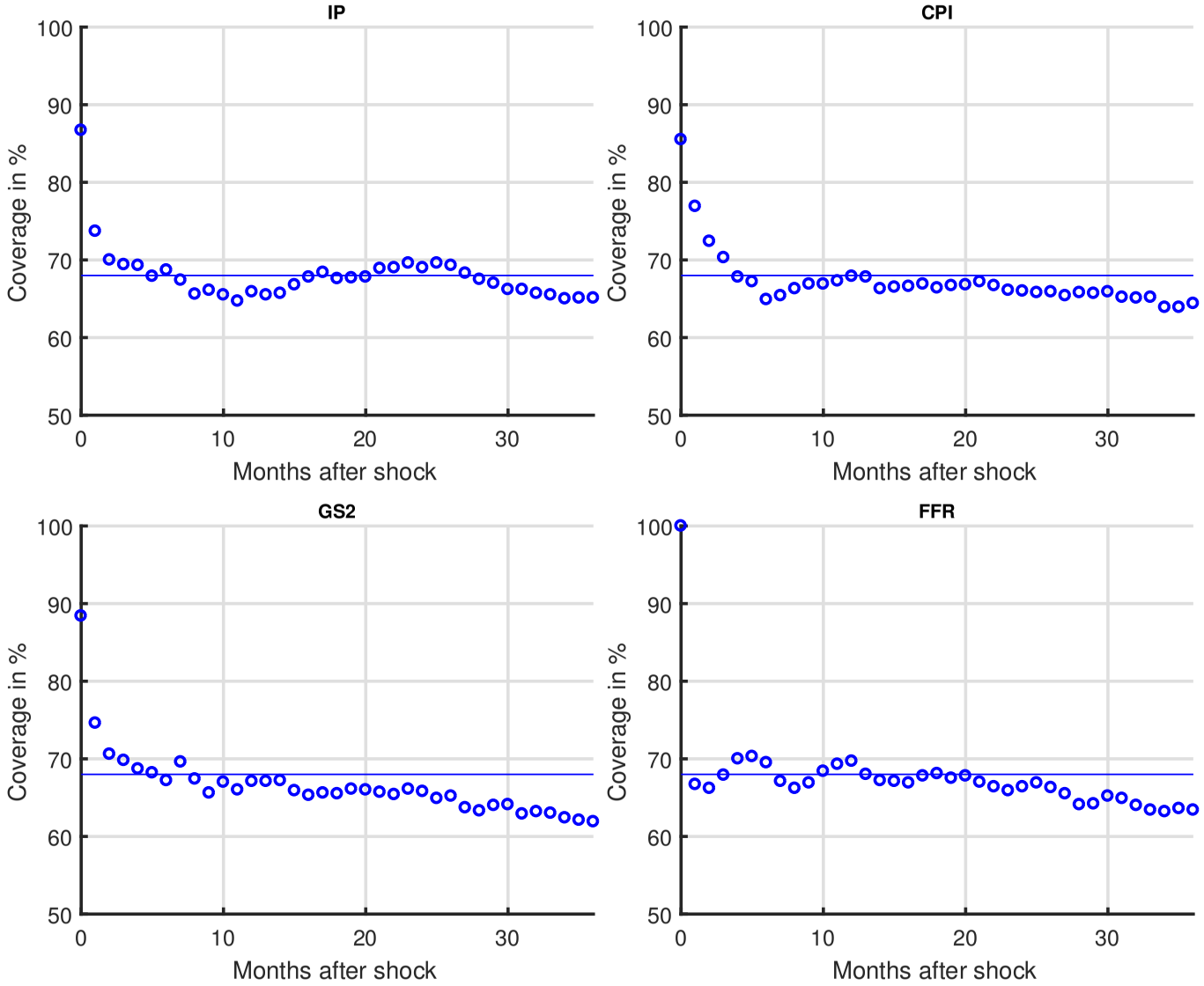

(Circles) Monte-Carlo estimate of the probability $P^*_\mu\Big([\underline{v}_{k,i,j}(\mu^*), \overline{v}_{k,i,j}(\mu^*)] \subset [\underline{v}_{k,i,j}(\widehat{\mu}_T) - .9945\widehat{\sigma}_{(k,i,j),T}/\sqrt{T}, \overline{v}_{k,i,j}(\widehat{\mu}_T) + .9945\widehat{\sigma}_{(k,i,j),T}/\sqrt{T} | Y_1, \ldots, Y_T]\Big)$ for the posterior distribution $\mu^* \sim \mathcal{N}(\widehat{\mu}_T, \widehat{\Omega}_T)$, with $T = 342$. The values $\widehat{\mu}_T$ and $\widehat{\Omega}_T$ correspond, respectively, to the estimators of the reduced-form parameter and its asymptotic covariance matrix in the UMP application. (Solid Line) Nominal credibility for the delta-method confidence interval (68%).

Figure 6: Projection Confidence Interval for CPI, IP, 2yTB, FF after the August 2010 announcement

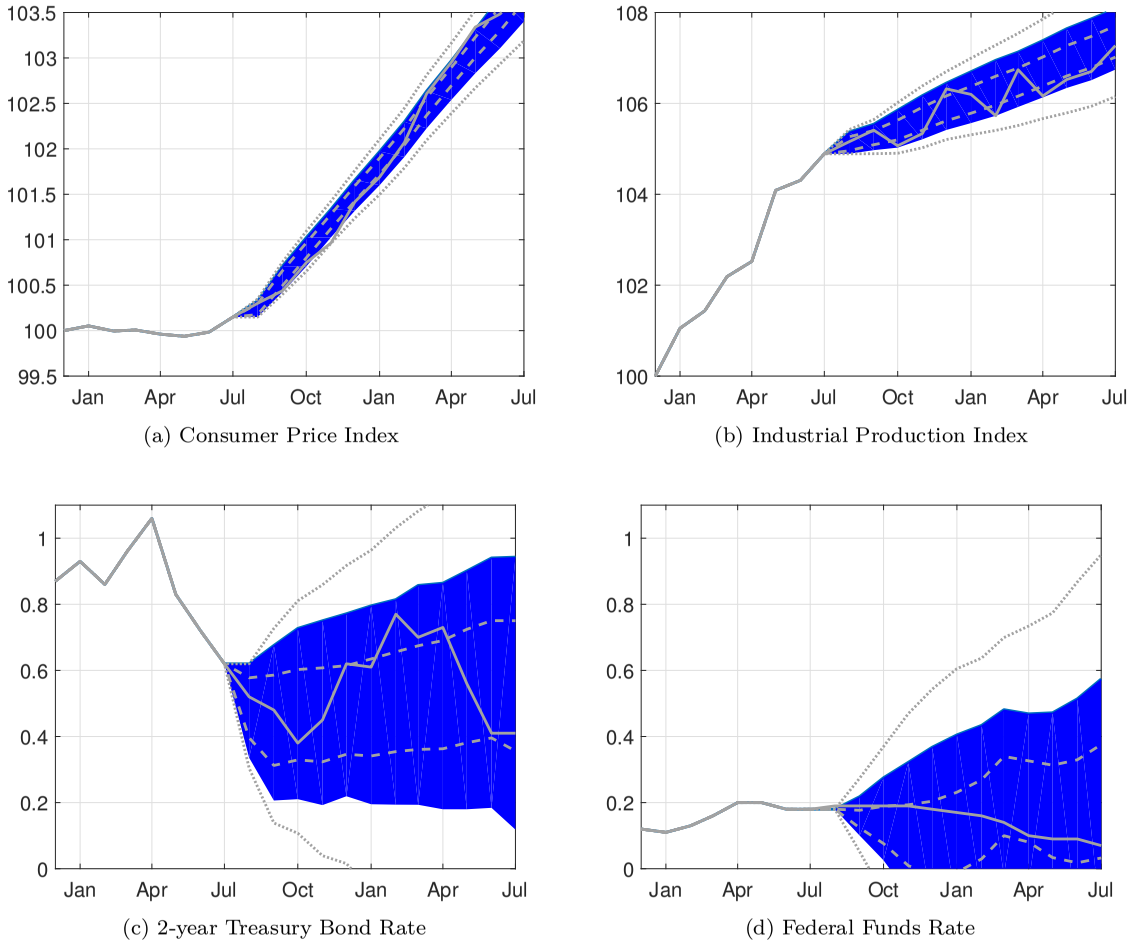

(a) Consumer Price Index

(b) Industrial Production Index

(c) 2-year Treasury Bond Rate

(d) Federal Funds Rate

(Shaded Area) Evolution of the Levels CPI, IP, 2yTB, and FF based on our 68% delta method confidence bands for the coefficients of Cumulative Impulse-Response Functions. (Solid Line) Observed Levels of CPI, IP, 2yTB, and FF from December 2009 to July 2011. Both the CPI index and the IP index were normalized to have a starting value of 100. (Dashed Line) 68% credible set constructed using the priors in Uhlig (2005). (Gray, Dotted Line) Gafarov et al. (2016)'s 68% confidence interval based on the projection approach.

Figure 7: Robust Credible Set for CPI, IP, 2yTB, FF after the August 2010 announcement

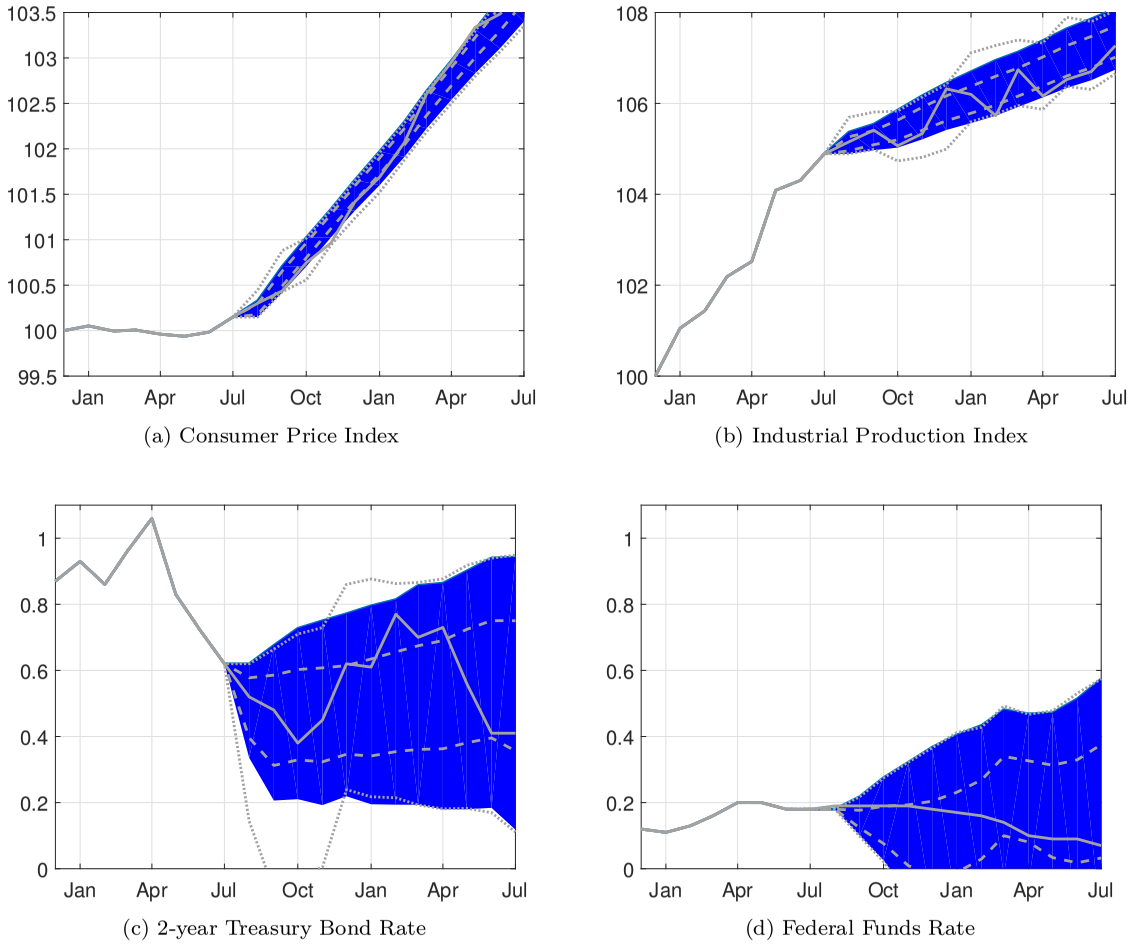

(a) Consumer Price Index

(b) Industrial Production Index

(c) 2-year Treasury Bond Rate

(d) Federal Funds Rate

(Shaded Area) Evolution of the Levels CPI, IP, 2yTB, and FF based on our 68% delta method confidence bands for the coefficients of Cumulative Impulse-Response Functions. (Solid Line) Observed Levels of CPI, IP, 2yTB, and FF from December 2009 to July 2011. Both the CPI index and the IP index were normalized to have a starting value of 100. (Dashed Line) 68% credible set constructed using the priors in Uhlig (2005). (Dotted Line) Giacomini and Kitagawa (2015)'s 68% robust-Bayes credible set constructed using the priors for the reduced-form parameters in Uhlig (2005)

Figure 8: Joint Credible Set (corresponding to all 4 variables and 36 horizons) for impulse response functions of CPI, IP, 2yTB, FF after the August 2010 announcement

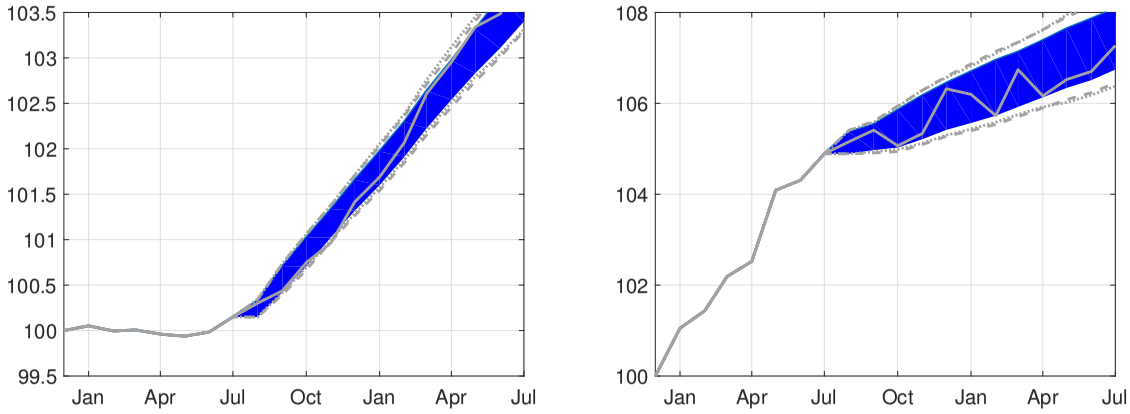

(a) Consumer Price Index

(b) Industrial Production Index

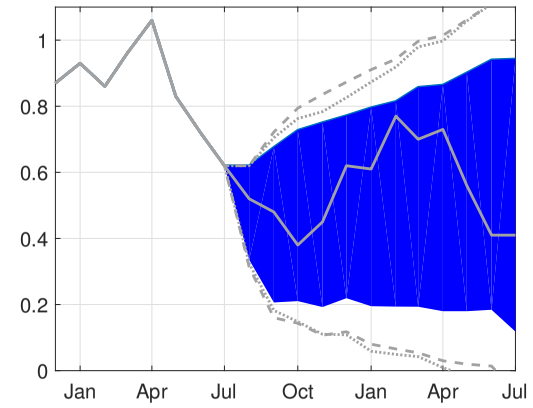

(c) 2-year Treasury Bond Rate

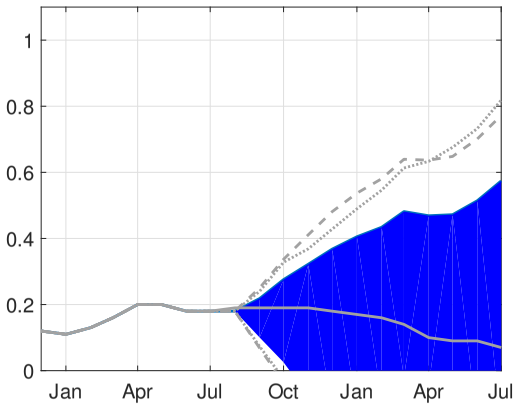

(d) Federal Funds Rate

(Shaded Area) Evolution of the Levels CPI, IP, 2yTB, and FF based on our 68% delta method confidence bands for the coefficients of Cumulative Impulse-Response Functions. (Solid Line) Observed Levels of CPI, IP, 2yTB, and FF from December 2009 to July 2011. Both the CPI index and the IP index were normalized to have a starting value of 100. (Dashed Line) Bonferroni-corrected joint 68% delta method confidence bands. (Dotted Line) Inoue and Kilian (2013)'s joint 68% Bayes credible set for impulse response functions using the priors for the reduced-form parameters in Uhlig (2005).

Figure 9: Confidence set for impulse response functions of CPI, IP, 2yTB, FF to a UMP shock under alternative identification scheme

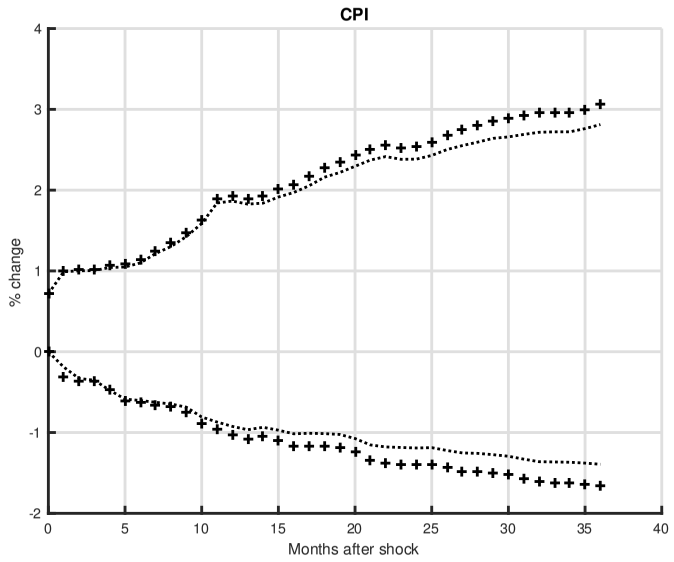

(a) Consumer Price Index

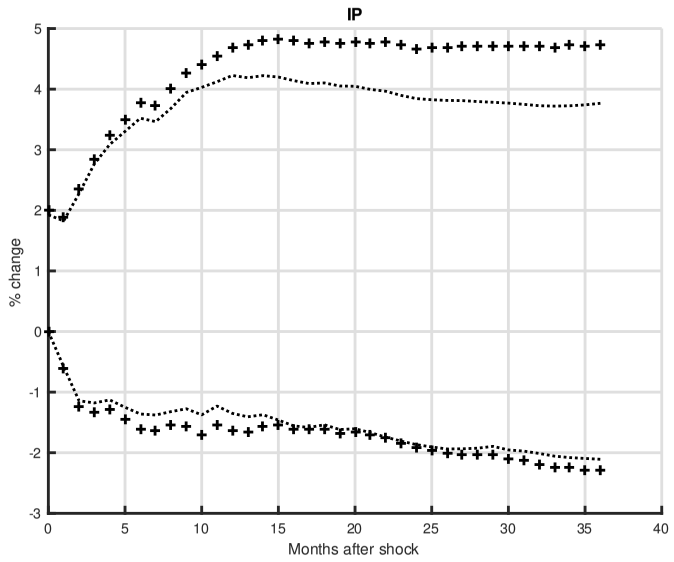

(b) Industrial Production Index

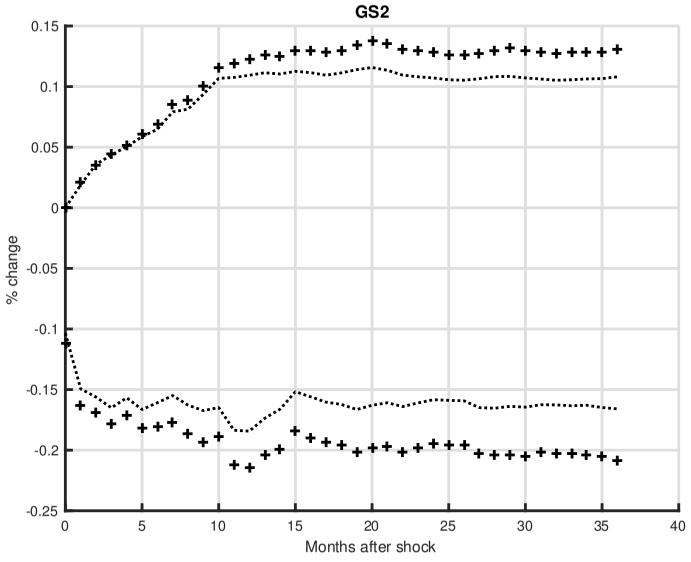

(c) 2-year Treasury Bond Rate

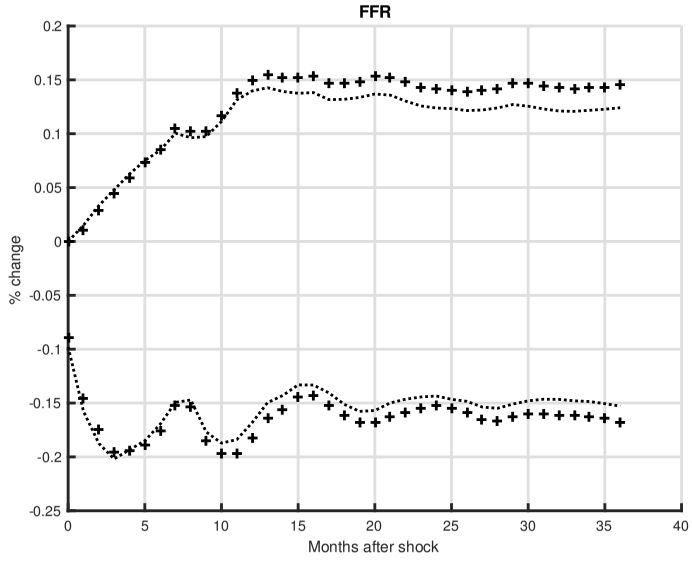

(d) Federal Funds Rate

(Pluses) 68% Bonferroni-type confidence bounds of Moon et al. (2013). See details on implementation in B.1.1 . (Dots) 68% delta method confidence bands

Note: the identification scheme used to produce these plots differs from the one used for Figure 1. The zero restriction on the response of the FFR is replaced with a negative sign restriction to improve the acceptance rate of the algorithm for Bonferroni-type CS.

Figure 10: The mathematical program defining $\overline{v}_{k,i,j}(\mu)$ $(n = 3)$ with one zero restriction.

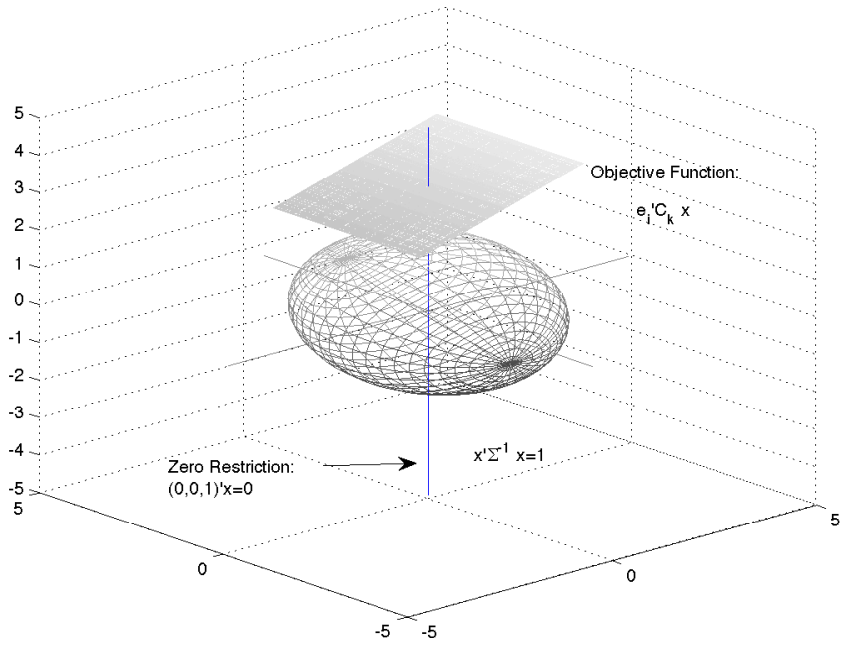

Figure 10 provides a graphical representation of the mathematical program (2.5), where $BB' = \Sigma$ has been replaced by the 'ellipsoid' constraint $x'\Sigma^{-1}x = 1$, $x \equiv B_j \in \mathbb{R}^3$. The objective function corresponds to the hyperplane with the normal vector $C_k(A)'e_i \in \mathbb{R}^3$. In this example, there is only one equality restriction with the normal vector given by the solid line. This restriction requires the contemporaneous impact of the j-th shock on the third variable to be zero. Note that without the equality restriction the maximizer and minimizer will be given by the point at which the hyperplane is tangent to the ellipsoid.

Figure 11: Solving for $\overline{v}_{k,i,j}(\mu)$ ($n = 3$, $\Sigma = \mathbb{I}_3$) with one equality restriction.

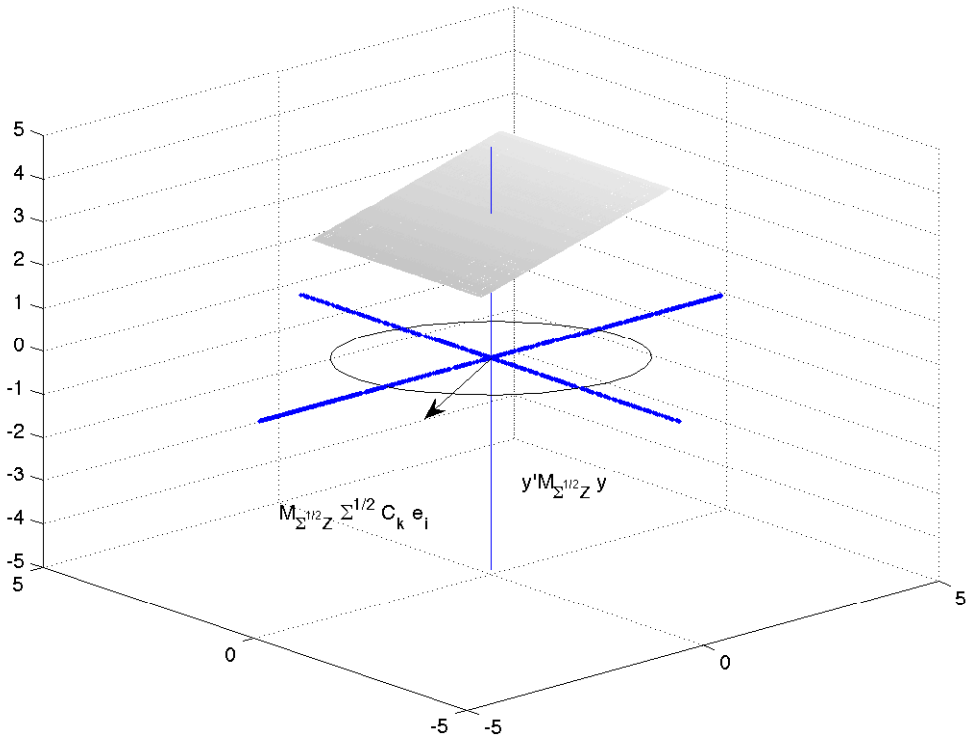

Figure 11 provides a graphical representation of the solution to the mathematical program (2.5) when $\Sigma = \mathbb{I}_3$ and there is only one zero restriction. The solution to the program must lie in the orthogonal complement of Z (the thin solid line). In this picture, the orthogonal complement corresponds to the space spanned by the thick solid lines. This implies that the rotated solution, denoted $\widetilde{x} \equiv \Sigma^{-1/2}x$, must be of the form $M_{\Sigma^{1/2}Z}y$ for some $y \in \mathbb{R}^3$. Hence, the only relevant part of $x'\Sigma^{-1}x = 1$ becomes the projected version of it: $y'M_{\Sigma^{1/2}}y = 1$, represented by the ellipsoid. One can find the value of this problem by projecting the gradient of the objective function on the orthogonal complement of $\Sigma^{1/2}z$ (the arrow) and selecting a direction in the ellipsoid collinear to it. The value function $\overline{v}_{k,ij}(\mu)$ will be given by the norm of the arrow.

Suppose there are only equality constraints. Note that $Z'B_j = \mathbf{0}_{m\times 1}$ implies that the re-parameterized choice variable $\widetilde{x} \equiv \Sigma^{-1/2}B_j$ must lie on the orthogonal space of $\Sigma^{1/2}Z$. That is, the selected value of $\widetilde{x}$ should be of the form:

$$\widetilde{x} = M_{\Sigma^{1/2}Z}y, \quad M_{\Sigma^{1/2}Z} \equiv \left(\mathbb{I}_n - \Sigma^{1/2}Z(Z'\Sigma Z)^{-1}Z'\Sigma^{1/2}\right), \ y \in \mathbb{R}^n.$$

The quadratic equality constraint also restricts the choice variable $\widetilde{x}$ to satisfy $\widetilde{x}'\widetilde{x} = 1$. Consequently, the problem can be re-written as

$$\max_{y\in\mathbb{R}^n} e_i'C_k\Sigma^{1/2}M_{\Sigma^{1/2}Z}y \quad \text{s.t.} \quad y'M_{\Sigma^{1/2}Z}y = 1.$$

An application of the Cauchy-Schwartz inequality shows that the positive value in $(A.1)$ gives the maximum response in (2.5).